中國土木水利工程學刊 第二十八卷 第二期 (民國一〇五年)
Journal of the Chinese Institute of Civil and Hydraulic Engineering, Vol. 28, No. 2, pp. 95–104, 2016
DOI : 10.6652/JoCICHE/2016-02802-03

ACCURACY ASSESSMENT OF PRECISE INDIRECT GEOREFERENCING FOR IMAGES OF UNMANNED AIRCRAFT SYSTEMS

Shih-Hong Chio

Department of Land Economics
National Chengchi University
Taipei, Taiwan 11605, R.O.C.

Key Words： VBS RTK GPS, bundle adjustment, aerial triangulation, UAS.

ABSTRACT

Unmanned Aircraft Systems (UASs) can collect high resolution and high quality images for local mapping. Before the UAS images can be used for accurate mapping tasks in local areas, the precise position and orientation of the UAS images should first be determined. Direct georeferencing by POS (Position and Orientation System), a combination of GPS (Global Positioning System) and IMU (Inertial Measurement Unit), is the best choice; however, most commercial UASs cannot carry highly accurate IMUs because of the limited payload. Therefore, this study will discuss the accuracy of indirect georeferencing for UAS images. One approach for indirect georeferencing is general aerial triangulation (AT) by using well-distributed ground control points (GCPs). The other one is GPS-supported AT with GPS observations as airborne controls. In this paper, the camera is calibrated by the field method, and the accuracy of these two approaches for indirect georeferencing is presented. Based on 20 horizontal check points and 29 vertical check points, this study shows the stereoscopic viewing accuracy of general AT for UAS images, collected by Canon EOS 5D Mark II camera with 24 mm F/1.4L II USM lens at a flying height of 550 m, is about 0.26 m (ca. 1.73 pixels) in planimetry and 0.27 m (ca. 1.80 pixels) in height. GPS-supported AT produced the stereoscopic viewing accuracy about 0.44 m (ca. 2.93 pixels) in planimetry and 0.55 m (ca. 3.67 pixels) in height. The test results show that the accuracy of these two indirect georeferencing approaches of fixed-wing UAS images can be used for updating local 1/5,000 topographic maps in Taiwan.

UAS 影像精確間接地理定位精度研究

邱式鴻

關鍵詞：虛擬基站即時動態定位、光束法平差、空中三角測量、無人飛行載具系統。

摘　要

無人飛行載具系統 UAS 可以蒐集高解析度和高品質的影像提供局部製圖。以 UAS 影像用來局部區域製圖時，UAS 影像必須先經精確定位定向。利用衛星定位系統 GPS 結合慣性導航單元 IMU 的定位定向 POS 系統執行直接地理定位是最佳的方法，然而受限於酬載能力，一般民間 UAS 無法酬載高精度的 IMU 執行直接定理定位。因此，本研究將討論 UAS 影像的間接地理定位精度。間接地理定位的第一個處理方法是完全使用分布良好的地

*通訊作者，國立政治大學地政學系副教授

面控制點，而不使用 GPS 觀測量做為空中控制的一般的空中三角測量平差 (簡稱空三平差)；另一個處理方法是則是使用 GPS 觀測量做為空中控制的 GPS 輔助空三平差。本文中，以野外率定場執行相機率定，並提出兩種 UAS 影像間接地理定位的精度。根據 20 個平面和 29 個高程檢核點檢核成果顯示，用 Canon EOS 5D Mark II 搭配 24 mm F/1.4L II USM 鏡頭於航高 550 公尺所蒐集的 UAS 影像，執行一般空三平差後的立體製圖平面精度 0.26 公尺 (約 1.73 像元)、高程 0.27 公尺 (約 1.80 像元)；而執行 GPS 輔助 UAS 影像空三平差後的立體製圖平面精度則為 0.44 公尺 (約 2.93 像元)、而高程精度為 0.55 公尺 (約 3.67 像元)。結果顯示兩種 UAS 影像間接地理定精度均能滿足台灣地區 1/5,000 地形圖之製圖精度要求。

1. INTRODUCTION

The UAV is an acronym for Unmanned Aerial Vehicle, which is an aircraft with no pilot on board. UAVs can be remote controlled aircraft (*e.g.* flown by a pilot at a ground control station) or can fly autonomously based on pre-programmed flight plans or more complex dynamic automation systems. The acronym UAV has been expanded in some cases to UAVS (Unmanned Aircraft Vehicle System). The FAA (Federal Aviation Administration) has adopted the acronym UAS (Unmanned Aircraft System) to reflect the fact that these complex systems include ground stations and other elements besides the actual air vehicles [1]. Nowadays, Unmanned aerial systems (UASs) are commonly used in military applications for recognition, environmental observation, maritime surveillance, and mine removal activities [2].

Compared with regular photogrammetric applications, UASs are a novel platform for carrying sensors and flying at required heights based on mission goals. UASs can carry optical sensors, thermal sensors, multispectral sensors and Lidar sensors [3,4]. Compared with traditional aerial vehicles, as UASs can fly at low altitude and on cloudy days to collect high resolution and high quality images, UAS technology for low altitude photogrammetric mapping can be further developed for the purpose of updating topographic products over specific local area [5], including orthoimages [6], topographic maps [7] and digital elevation models [8].

In order to achieve accurate photogrammetric mapping requirement, no matter traditional aerial vehicle or UAS was employed, aerial images should firstly be positioned and oriented. Normally two approaches including direct and indirect georeferencing can be adopted. Direct georeferencing employs GPS/IMU (Inertial Measurement Unit) instruments, *i.e.* POS (Position and Orientation System) systems, to determine the exterior orientation parameters of UAS images by post-processing mode. Conversely, if the position and orientation of images are determined by performing aerial triangulation (AT) by using ground control points (GCPs) or airborne controls [12], it is called indirect georeferencing methodology.

Although some studies have focused on direct georeferencing of UAS images [10,11], it is realized that most commercial UASs cannot carry highly accurate IMUs due to the limited payload. Therefore, indirect georeferencing method becomes the main approach for accurate mapping tasks using UAS images.

To carry out this indirect georeferencing approach, it is essential to survey the appropriate number of control points, including GCPs and airborne controls from GPS observations. Then the corresponding image coordinates of GCPs and the imaging points of the same object points in the overlap areas between adjacent aerial images, *i.e.* tie points, should be measured manually or automatically. Together with the accurate camera parameters, they are used simultaneously to determine the exterior parameters of UAS images and the 3-D coordinates of tie points by using the least squares method based on collinearity equations [12], which is known as the bundle adjustment AT. Two approaches can be adopted for bundle adjustment AT. One approach is called general AT without GPS observations as airborne controls. The other one is called GPS-supported AT with GPS observations as airborne controls. When performing GPS-supported AT, GPS observations are introduced in a combined block adjustment as eccentric observations [13] of the positions of the camera projective center. With a small number of GCPs for geodetic control, GPS-supported AT can substantially reduce the demands on GCPs based on the previous studies on AT [14-16]. Table 1 shows the pros and cons of general AT, GPS-supported AT and direct georeferencing of UAS images.

Table 1 Pros and cons of the general AT, GPS-supported AT and direct georeferencing of UAS images

Items	Indirect georeferencing: general AT	Indirect georeferencing: GPS-supported AT	direct georeferencing
Ground controls	Well-distributed ground control points	At least one ground control points in each corner of block	Unnecessary in theory
Additional devices on UAS	No	Yes, double-frequency GPS receiver	Yes, POS (GPS + IMU) system
Multi-path and interference	No	Yes	Yes
Costs for ground survey	expensive	Inexpensive	No
Time-saving	No	Yes	Yes

Therefore, this study will present our tests related to the accuracy of indirect georeferencing for UAS images, in which general bundle adjustment AT and GPS-supported bundle adjustment AT is conducted respectively. Precisely measured ground points are used as check points for evaluating the accuracy of these two indirect georeferencing approaches. In addition to the root mean square errors (RMSEs) of ground check points, the accuracy of stereo viewing will also be applied to examine the potential of stereo mapping for 1/5,000 maps using these two indirect georeferencing approaches. Section II presents the theories and methods related to the indirect georeferencing approach, including camera calibration and AT. Section III describes the tests and offers the discussion. Section IV offers conclusions.

2. THEORIES AND METHODS OF INDIRECT GEOREFERENCING METHODOLOGY

2.1 Camera Calibration

Because of commercial UAS payload limitations, only non-metric cameras can be installed. Non-metric cameras use low-cost lenses and provide autofocus functions. To meet accurate indirect georeferencing demands, non-metric cameras should first be calibrated. When the camera is calibrated, the autofocus function should be disabled in order to fix the focus length. Otherwise, the UAS images will be taken by different imaging principal distance and it will make the camera calibration difficult or failed. Additionally, the calibration of the lens of a camera for aerial photogrammetric application is required at infinity focus, thus, the field method [12] is suitable to be adopted for camera calibration. The calibration principle is basically an extension of the mathematical bundle adjustment model, called self-calibration bundle adjustment. The basic collinearity equation is augmented by additional terms, Δx and Δy, in Eq. (1) to formulate the basic camera calibration equation:

$$x_a - x_0 + \Delta x = -f\frac{m_{11}(X_A - X_L) + m_{12}(Y_A - Y_L) + m_{13}(Z_A - Z_L)}{m_{31}(X_A - X_L) + m_{32}(Y_A - Y_L) + m_{33}(Z_A - Z_L)}$$
$$y_a - y_0 + \Delta y = -f\frac{m_{21}(X_A - X_L) + m_{22}(Y_A - Y_L) + m_{23}(Z_A - Z_L)}{m_{31}(X_A - X_L) + m_{32}(Y_A - Y_L) + m_{33}(Z_A - Z_L)} \quad (1)$$

x_a, y_a : The photo coordinates of point A
x_0, y_0 : The principal point coordinates
$\Delta x, \Delta y$: Additional terms for the point photo coordinates
f : The focal length of the lens
X_A, Y_A, Z_A : The object space coordinates of point A
X_L, Y_L, Z_L : The object space coordinates of the exposure station
m_{ij} : The elements of rotation matrix formed by rotation angles

The Δx and Δy terms consist of various additional parameters based on different models. This study will use SOCKET SET Orientation Management (SOCKET SET ORIMA) photogrammetric software for camera calibration, which adopts the Brown physical model [17]. Equation (2) denotes the Brown mathematical model that was originally developed for frame camera calibration.

$$\begin{aligned}\Delta x &= x_0 + x\left[a_1(r^2 - r_0^2) + a_2(r^4 - r_0^4) + a_3(r^6 - r_0^6)\right] + b_1 x + b_2 y \\ &\quad + \frac{x}{c}\left[c_1(x^2 - y^2) + c_2 x^2 y^2 + c_3(x^4 - y^4)\right] + d_1 xy + d_2 y^2 \\ &\quad + d_3 x^2 y + d_4 xy^2 + d_5 x^2 y^2 \\ \Delta y &= y_0 + y\left[a_1(r^2 - r_0^2) + a_2(r^4 - r_0^4) + a_3(r^6 - r_0^6)\right] \\ &\quad + \frac{y}{c}\left[c_1(x^2 - y^2) + c_2 x^2 y^2 + c_3(x^4 - y^4)\right] + d_6 xy + d_7 x^2 \\ &\quad + d_8 x^2 y + d_9 xy^2 + d_{10} x^2 y^2\end{aligned} \quad (2)$$

$\Delta x, \Delta y$: The correction of image point coordinate observations
x_0, y_0 : The principal point coordinates
c : The calibrated focal length
r, r_0 : The radial distances from the measured point to the image center and the principal point, respectively
a_1, a_2, a_3 : The radial lens distortion polynomial coefficients
b_1, b_2 : The affinity and non-orthogonality of the image system
c_1, c_2, c_3 : The non-flatness of the image plane
$d_1, \ldots, d_{10}$: Regular and irregular film deformations

As the lens distortion mainly results from the radial distortion [18], the set of radial lens distortion parameters (a_1, a_2, a_3) listed in Eq. (2), together with the calibrated focal length (c), principal point coordinates (x_0, y_0), are introduced in the camera calibration task to be determined in this study.

When performing camera calibration using the field method, two equations combined with Eqs. (1) and (2) can be formed for each pair of image points, in which unknowns are all exterior parameters of images, calibrated camera parameters, and ground 3-D coordinates of terrain tie points. With proper GCP configuration, camera calibration solutions are determined based on the least squares method after the related weights of the image point observations and GCPs are given. Because photogrammetric software, SOCKET SET ORIMA, is used for camera calibration, automatic and manual tie point measurement and blunder detection is also performed by using this photogrammetric software. Wolf and Dewitt [12] described the adjustment principle in more detailed. The RMSEs of ground check points in the E, N and H directions are used to verify the quality of camera calibration.

2.2 Aerial Triangulation (AT)

To evaluate the performance of indirect georeferencing using UAS images, bundle adjustment with and without GPS support, that is general AT and the GPS-supported AT, are carried out in this study. For the processing, the SOCKET

SET ORIMA photogrammetric software is applied. The basic theory of general AT and the GPS-supported AT is shortly described as the following subsections 2.2.1 and 2.2.2.

2.2.1 General AT

For general AT using the proper GCP configuration, two basic coordinate observation equations for each image point based on Eq. (1) can be formed for each ray after the systematic error Δx, Δy for x, y coordinates are corrected. Unknowns are all exterior parameters of images, and the ground 3-D coordinates of terrain tie points, the solutions are determined by indirect observation adjustment based on the least squares method after the related weights of the image point observations and GCPs are given. The GCPs are basically allocated according to the traditional configurations for aerial photogrammetry by using the metric camera. However, using GPS techniques to collect 3-D GCP control information is fast and easy. Some modification will be made in this study. It means all the GCPs are full controls. Meanwhile, natural points, instead of artificial targets, are selected as full control points. Similarly, after finishing general AT, the RMSEs of check points in the *E*, *N* and *H* directions are used to verify the accuracy of general AT.

2.2.2 GPS-supported AT

(1) GPS Observation Equations

For GPS-supported AT, any GPS observations interpolated from an accurate trajectory based on the exposure time and GPS recorded time are corresponding to the antenna phase center. The phase center of the antenna and the rear nodal point of the aerial camera lens cannot occupy the same point in space [19]. For traditional aerial vehicles, this offset can be surveyed by terrestrial surveying techniques, such as the free station method using the total station instrument [20], by using fiducial marks as controls. This offset, which is based on the fiducial coordinate system, is then transformed into the offset based on the ground coordinate system [21]. However, a charge coupled device (CCD) or complementary metal oxide semiconductor (CMOS) sensor used by the non-metric camera for recording the image data is not of fiducial marks and is also too small to make precise offset surveys by total station instrument. Compared to conventional GPS-supported AT, this study should overcome this problem. Only Hinsken *et al*. [22] used the constant parameters in drift parameters to survey the GPS antenna-camera offset and to decrease the influence of system errors caused by GPS antenna-camera offset. Therefore, GPS antenna-camera offset problems in the sensor system can be solved by including drift parameters in the bundle adjustment. Blankenberg [23] also stated that drift parameters can be used to solve problems caused by inaccurate determination of cycle ambiguity because of cycle slips during the kinematic positioning process, and to overcome the systematic error caused by inaccurately surveying GPS antenna-camera offset.

Additionally, according to Ackerman [24], a photogrammetric camera equipped with a shutter synchronized electronic signal should provide accuracy better than 1 ms for GPS-supported AT. In this study, GPS observations will be obtained from flying trajectories by interpolation based on GPS times and the exposure time of UAS images to support AT of UAS images; it is impossible to make the difference between the GPS time and imaging exposure time less than 1 ms for the UAS. If the time difference is 10 ms, the interpolation error is about 0.3 m, based on a UAS speed of approximately 100 km/h. According to Blankenberg [23], time shifts and interpolation error can be also eliminated by adding drift parameters.

In addition to the abovementioned advantages, some errors can be compensated through drift parameters, such as various systematic geodetic data. The 3-D coordinate system for GPS observations is based on the World Geodetic System 1984 (WGS84), however, the horizontal mapping coordinate system is a projection system, such as Taiwan Datum 1997 (TWD97), and the vertical data mapping system is the Taiwan Vertical Datum 2001 (TWVD2001). The data differences between the GPS and mapping system can be transformed by fewer GCPs, and drift parameters can compensate for the system error caused by this transformation [24].

The drift parameters can also be attributed to the uncertainties in the a priori corrections (*e.g.*, atmospheric refraction) and unmodelled error effects (*e.g.*, satellite orbit errors), despite applying various techniques. During a time interval, such as 10 to 15 min, this drift error is approximately linear [16]. Therefore, six parameters can be used to model these systematic errors: three constant parameters and three time-dependent parameters per strip. That is, including the stripwise linear drift parameters allows for compensation of these systematic errors. Six linear unknown parameters per strip (three offsets and three drifts) are added to the exposure station observation equations to manage the systematic errors introduced by the GPS measurements. In this study, the six linear drift parameters per strip will be estimated during bundle adjustment AT based on the GPS values from interpolating the flying trajectory data collected by the Virtual Base Station Real Time Kinematic Positioning (VBS RTK) GPS technique. As the horizontal accuracy of the present VBS RTK GPS is about 2 cm, and the elevation accuracy is about 5 cm [25]; therefore, the interpolated GPS values are treated as observations; thus, the GPS observation equation is represented by Eq. (3) [22]:

$$\begin{bmatrix} X_i^{GPS} \\ Y_i^{GPS} \\ Z_i^{GPS} \end{bmatrix} + \begin{bmatrix} V_{Xi}^{GPS} \\ V_{Yi}^{GPS} \\ V_{Zi}^{GPS} \end{bmatrix} = \begin{bmatrix} X_i^{PC} \\ Y_i^{PC} \\ Z_i^{PC} \end{bmatrix} + \begin{bmatrix} aX \\ aY \\ aZ \end{bmatrix} + \begin{bmatrix} bX \\ bY \\ bZ \end{bmatrix} \times (t - t_0) \qquad (3)$$

$X_i^{GPS}, Y_i^{GPS}, Z_i^{GPS}$: *GPS* observations corresponding to image *i*

$V_{Xi}^{GPS}, V_{Yi}^{GPS}, V_{Zi}^{GPS}$: Residuals for $X_i^{GPS}, Y_i^{GPS}, Z_i^{GPS}$ observations

$X_i^{PC}, Y_i^{PC}, Z_i^{PC}$: Coordinates of camera perspective center *i*

aX, aY, aZ : Three linear drift constant parameters of a strip in object space

bX, bY, bZ : Three time-dependent linear drift parameters of a strip in object space

$(t - t_0)$: The time difference between exposure time t of image i and strip beginning time t_0

(2) Solutions to GPS-supported Bundle Adjustment

While performing VBS RTK GPS-supported bundle adjustment AT of UAS images, two image point coordinate observation equations based on Eq. (1) can be formed for each ray after the systematic error Δx, Δy for x, y coordinates are corrected. Three GPS observation equations for each image were obtained by using Eq. (3). Unknowns are all exterior parameters of UAS images, the six linear drift parameters for each strip and the 3-D coordinate of terrain tie points. For GPS-supported AT, the highly accurate GPS observations can be regarded as control points, similar to GCPs in the air. Ideally, GPS-supported AT does not require any GCPs. However, the WGS84 coordinate system is used for the GPS positioning results and national reference systems, such as TWD97 and TWVD2001 in Taiwan, are generally used as mapping coordinate systems. It is necessary to transform the WGS84 coordinates into the mapping coordinate system. Therefore, at least three GCPs are necessary to transform the data. The unknown linear drift parameters introduce the problem of singularities. The six linear parameters per strip destabilize the block geometry, and may negatively affect the recovery of all unknowns in the adjustment (*e.g.*, normal matrix singularity). Two approaches can be used to avoid singularities [24]: adding two vertical control point chains or flying two cross strips. To reduce the number of the GCPs, flying two cross strips with 8 GCPs is used in this study. Additionally, the surveying of 3-D GCP control information by GPS techniques is currently fast and easy; therefore, the GCP configuration proposed by Ackermann [24] was modified for the tests in this study. Full control points replace the horizontal and vertical control points and the GCPs are located on the strip overlaps for stronger control geometry.

For the GPS-supported AT using the proper GCP configuration, the solutions are determined by indirect observation adjustment based on the least squares method, after the related weights of the image point observations and control points, including GCPs and airborne controls, are given. The detailed adjustment principle was described by Wolf and Dewitt [12]. The accuracy of VBS RTK GPS-supported AT for UAS images is verified by calculating the RMSEs of the check points in the E, N and H directions.

3. EXPERIMENTS AND DISCUSSION

The used fixed-wing UAS and the related devices installed on UAV in this study is illustrated as Fig. 1, where Trimble BD970 GNSS OEM is installed to collect $L1$/$L2$ carrier phase data to capture highly accurate and precise flying trajectories by using the VBS RTK GPS technique. The post-processing approach from the e-GPS service provided by the

(a) DoDo Pro fixed-wing UAV and the related devices installed on the UAV

(b) Ground control station

Fig. 1 DoDo Pro fixed-wing UAS

National Land Surveying and Mapping Center (NLSC) in Taiwan is used. The non-metric camera used is Canon EOS 5D Mark II digital camera with 24 mm f/1.4L II USM lens and CMOS chips are employed for recording the image data; the pixel size is 6.4 μm and the image size is 5,616 pixels × 3,744 pixels. The setting for shutter speed is 1/2,000 s and the f-stop is 3.2. Meanwhile the setting for ISO is automatic.

3.1 Result of Camera Calibration

This subsection describes the results of the camera calibration conducted by using the calibration field established by the NLSC at Nantou County in central Taiwan. The used UAS images were taken on October 2, 2012. The relevant information from the data used for camera calibration is shown in Table 2. The 3-D coordinates for the ground calibration targets were surveyed by using the static GPS surveying technique. The 3-D coordinates of WGS84 system were converted into horizontal E and N mapping coordinates in the TWD97 system and the height H coordinate remained in the ellipsoid height system.

The photogrammetric software, SOCKET SET ORIMA, was used for the self-calibration bundle calibration. Before performing self-calibration bundle calibration, the weights of image point observations were set based on a measurement accuracy of 6.4 μm, and the weights of GCPs were set according to their corresponding accuracies: 0.02 m, 0.02 m and 0.05 m in the E, N and H directions, respectively. The camera parameters used for calibration included the calibrated focal length (c), principal point coordinates (x_0, y_0) and radial lens distortion (a_1, a_2, a_3). The main processing steps of self-calibration bundle adjustment include: (1) initial camera parameter inputs, (2) automatic tie point extraction, (3) free net

Table 2 The related information of used data for camera calibration by field method

Info.	Description	Info.	Description
No. of Strip	6		
No. of UAS images	95	Average ground elevation (orthometric height)	190 m
Forward overlap	80%	Ground sampling resolution	0.15 m
Side overlap	55%	No. of full control points	33
Flying height	550 m	No. of check points	11

adjustment, (4) automatic or manual blunder detection, (5) tie point manual measurement and deletion, (6) image point measurement of GCPs and (7) self-calibration bundle adjustment for camera calibration. Approximately 1800 terrain tie points remained after blunder detection by using 95 UAS images in six strips. The sigma naught by using 33 GCPs is 6.6 μm. The GCPs configuration (see Fig. 2) is based on conventional aerial photogrammetry. The RMSEs of the 11 check points (see Fig. 3) in E, N and H coordinate components are 0.08 m, 0.07 m and 0.14 m, respectively. It corresponds to 0.71 pixels in planimetry and 0.93 pixels in height. The average of coordinate difference in E, N and H coordinate components are −0.03 m, −0.02 m and −0.06 m, respectively. This indicates high quality camera calibration. Table 3 shows the calibrated camera parameters.

If all the parameters in Brown mathematical model (see Eq. (2)), including the principal point coordinates (x_0, y_0), the calibrated focal length (c), the radial lens distortion (a_1, a_2, a_3), the affinity and non-orthogonality of the image system (b_1, b_2), the non-flatness of the image plane (c_1, c_2, c_3), and regular and irregular film deformations (d_1, …, d_{10}), are simultaneously used for calibration, the RMSEs of the same 11 check points (see Fig. 3) in E, N and H coordinate components are 0.07 m, 0.06 m and 0.13 m, respectively. Compared with the check results by only using the calibrated focal length (c), principal point coordinates (x_0, y_0) and radial lens distortion (a_1, a_2, a_3), it shows only 1 cm difference in the E, N and H coordinate components. Therefore, it also demonstrates the photo coordinate corrections are mainly from principal point coordinates (x_0, y_0) and radial lens distortion (a_1, a_2, a_3). It also proves that calibrated focal length (c), principal point coordinates (x_0, y_0) and radial lens distortion (a_1, a_2, a_3) are the main parameters for calibration.

3.2 Results of Indirect Georeferencing

The test was conducted on approximately 300 ha in Jian Township, Hualien County, Taiwan. The test UAS images were captured at a flying height of approximately 550 m. The imaging resolution is approximately 15 cm/pixel. In total, 266 UAS images in 9 strips, including 2 cross strips, were collected with an 80% image forward overlap and a 45% image sideoverlap for tests. The 3-D GCP coordinates and check points were surveyed by using the VBS RTK GPS technique. The surveyed ellipsoid height was converted to the orthometric height in TWVD2001 based on five points with known orthometric height surrounding the test site, using a Classical 3D Transformation in SKIP Pro software.

Table 3 Calibrated camera parameters

Camera Parameters		Values
Calibrated Focal Length (mm)		24.6596
Principal Point Offsets (x_0 (mm) , y_0 (mm))		(0.2094, 0.1269)
Radial lens distortion	a_1 (mm^{-2})	−0.112E-03
	a_2 (mm^{-4})	0.268E-06
	a_3 (mm^{-6})	−0.193E-09

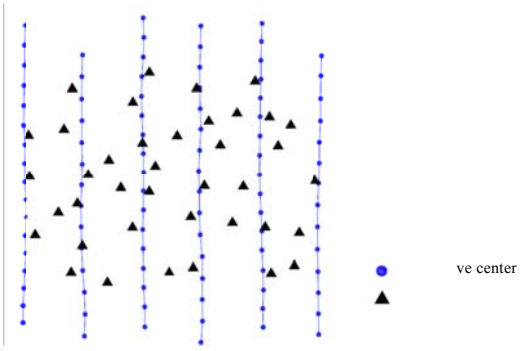

Fig. 2 The configuration of GCPs for field calibration

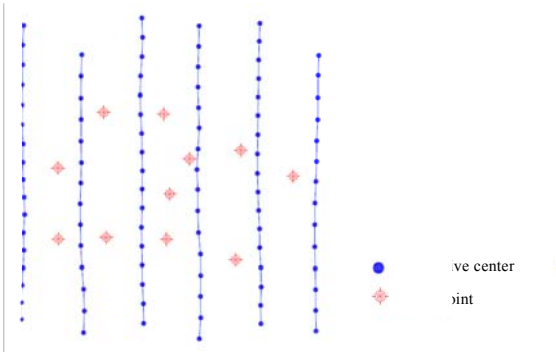

Fig. 3 The distribution of check points for field calibration

The photogrammetric software, SOCKET SET ORIMA, was used for general AT and GPS-supported AT. A total of 204 UAS images in 7 strips was used for general AT and 266 UAS images in 9 strips, including 2 cross strips, were used for GPS-supported AT. While performing AT, the weights of image point observations were set according to a measurement accuracy of 6.4 μm. The weights of GCPs and GPS observations for AT were set according to their corresponding accuracies (0.05 m, 0.05 m and 0.1 m). All terrain tie points on the images were extracted by using automatic matching methods. Blunder detection and manual tie point measurement was conducted by using the same photogrammetric software.

For the test of general AT, Fig. 4 shows the configuration of 28 GCPs and the distribution of the 6 check points. After blunder detection, about 4700 terrain tie points remained. The sigma naught is 6.7 μm and the RMSEs of 6 ground check points are 0.16 m, 0.17 m and 0.37 m in E, N and H,

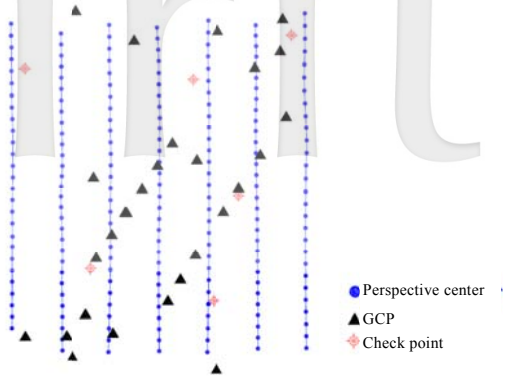

Fig. 4 Distribution of 28 GCPs and 6 check points for the general AT

respectively (see Table 4). The planimetric accuracy is about 0.23 m. It corresponds to 1.53 pixels in planimetry and 2.47 pixels in height, respectively. The result verifies the applicability of the camera parameters calibrated by field method.

For the test of GPS-supported AT, the accurate flying trajectory for 1 Hz was collected by a post-processing approach. The GPS observations corresponding to the image exposure time were then interpolated by using the image exposure time and GPS time to provide highly accurate aerial control information for GPS-supported AT. Figure 5 shows the configuration of GCPs, namely two cross strips with 8 GCPs, and the distribution of the 6 check points. All GCPs are located on the strip overlap. Because the strip overlap in the bottom right corner is the river, the locations of GCPs in the river are set toward the left.

After blunder detection, approximately 6000 terrain tie points remained. After AT, the sigma naught is 11.2 μm; Table 5 shows that the RMSEs of the six check points in the *E*, *N* and *H* coordinate components are 0.08 m, 0.22 m and 0.59 m, respectively. The planimetric accuracy is about 0.23 m. It corresponds to 1.53 pixels in planimetry and 3.93 pixels in height, respectively. This reflects obvious systematic error in *H* component, but still verifies the applicability of the linear drift parameters for VBS RTK GPS-supported AT.

If GPS observations are directly used as the observation of perspective centers, the RMSEs of the 6 check points in the *E*, *N* and *H* coordinate components are 0.24 m, 0.29 m and 1.73 m, respectively. The test indicates that linear drift parameters can overcome GPS antenna-camera offset problems.

3.4 Accuracy Evaluation of Stereoscopic Viewing

For further discussion of the accuracy of these two indirect georeferencing approaches, the check results of stereoscopic viewing are listed in Tables 6 and 7. Figures 6 and 7 show the distribution and the difference vector of 20 horizontal ground check points and 29 vertical ground check points of stereoscopic viewing based on the results of general AT and GPS-supported AT. The coordinates of horizontal and vertical ground check points are surveyed by the VBS RTK GPS in real time, and also measured by stereoscopic viewing using stereo images with 60% end lap in each strip. The coordinates of horizontal and vertical check points surveyed by the VBS RTK GPS. The surveyed ellipsoid

Table 4 Check results of the general AT

	Coordinate difference (Unit: meter)		
Pt.	*E*	*N*	*H*
HLCH03	–0.19	–0.03	–0.02
HLCH04	0.20	–0.26	–0.65
HLCH07	0.25	0.22	–0.37
HLCH09	0.06	–0.21	0.42
HLCH010	0.03	–0.06	0.08
L06	0.06	0.02	0.30
Average	**0.07**	**–0.05**	**–0.04**
RMSEs	0.16	0.17	0.37

Table 5 Check results of VBS RTK GPS-supported AT

	Coordinate difference (Unit: meter)		
Pt.	*E*	*N*	*H*
L06	–0.07	–0.24	–0.48
L17	0.07	–0.09	–0.55
L23	0.11	–0.21	–1.16
L28	0.10	–0.34	–0.08
FHLCH9	0.05	–0.05	–0.15
FHLCH17	–0.04	0.25	0.15
Average	**0.04**	**–0.11**	**–0.38**
RMSEs	0.08	0.22	0.59

Table 6 The statistics of check results for stereoscopic viewing from the general AT (Unit: Meter)

	Horizontal check points		Vertical check points
No.	20		29
	Δ*E*	Δ*N*	Δ*H*
Average	**–0.10**	**–0.14**	**0.02**
Max.	0.28	0.09	0.66
Min.	–0.39	–0.48	–0.30
RMSEs	0.17	0.19	0.27

Table 7 The statistics of check results for stereoscopic viewing from GPS-supported AT (Unit: Meter)

	Horizontal check points		Vertical check points
No.	20		29
	Δ*E*	Δ*N*	Δ*H*
Average	**–0.12**	**0.04**	**0.21**
Max.	0.34	0.59	1.06
Min.	–0.66	–0.75	–0.86
RMSEs	0.33	0.29	0.55

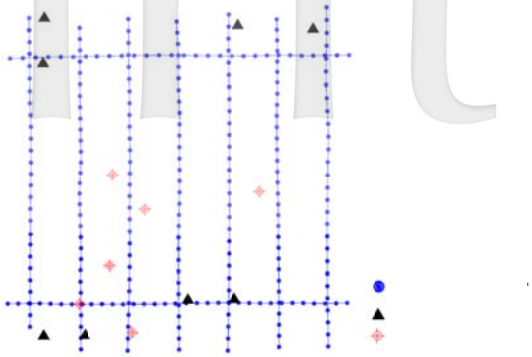

Fig. 5 Distribution of 8 GCPs and 6 check points for GPS-supported AT

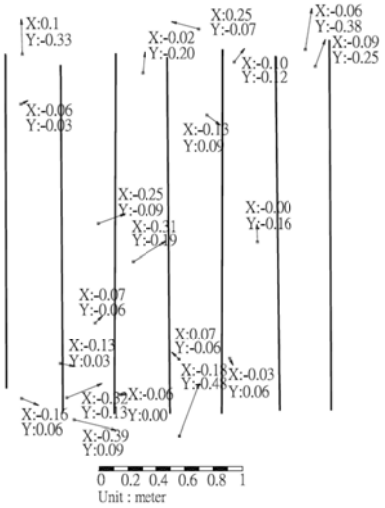

(a) Horizontal check points

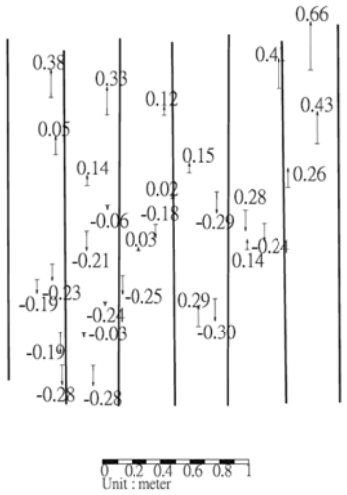

(b) Vertical check points

Fig. 6 Difference vectors of check points for stereoscopic viewing based on the results of general AT

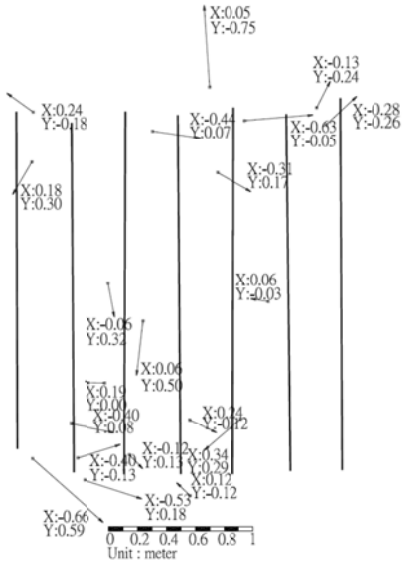

(a) Horizontal check points

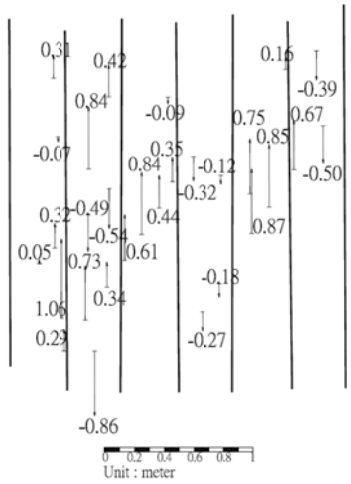

(b) Vertical check points

Fig. 7 Difference vectors of check points for stereoscopic viewing based on the results of GPS-supported AT

height was converted to the orthometric height in TWVD2001 by using the same approach to the 6 check points in AT. The RMSEs of check points from stereoscopic viewing can reach 0.26 m (ca. 1.73 pixels) in planimetry and 0.27 m (ca. 1.80 pixels) in height using general AT. The RMSEs of check points from stereoscopic viewing using GPS- supported AT can reach 0.44 m (ca. 2.93 pixels) in planimetry and 0.55 m (ca. 3.67 pixels) in height. In Taiwan, the planimetric accuracy requirement for 1/5,000 topographic maps is 1.25 m and the vertical accuracy requirement for 1/5,000 topographic maps is 1 m in normal terrain [26]. Therefore, even the check results of stereo viewing still remain systematic error, especially in *E* and *N* coordinate components using the results of general AT and in *E* and *H* coordinate components using the results of VBS RTK GPS-supported AT, the test results still show that the accuracy of these two indirect georeferencing approaches of fixed-wing UAS images can be used for updating local 1/5,000 topographic maps in Taiwan.

4. CONCLUSIONS

In this paper, the accuracy of the two approaches for indirect georeferencing is presented. This study shows that the accuracy of general AT for UAS images, collected by Canon EOS 5D Mark II camera with 24 mm *F*/1.4*L* II USM lens at a flying height of 550 m, is about 0.23 m (1.53 pixles) in planimetry and 0.37 m (2.47 pixels) in height, based on the 6 check points. Additionally, a Trimble BD970 GNSS OEM is carried on the UAS to collect *L*1/*L*2 carrier phase data for capturing highly accurate and precise flying trajectories by using the VBS RTK GPS technique. GPS observations are then interpolated based on image exposure times as airborne controls to support AT of UAS images. GPS-supported AT produced accuracy about 0.23 m (1.53 pixels) in planimetry and 0.59 m (3.93 pixels) in height, based on the 6 check points. Based on 20 horizontal check points and 29 vertical check points, this study shows that the stereoscopic viewing accuracy about the results of general AT for UAS images, collected by Canon EOS 5D Mark II camera with 24 mm *F*/1.4*L* II USM lens at a flying height of 550 m, is about 0.26 m (ca. 1.73 pixels) in planimetry and 0.27 m (ca. 1.80 pixels) in height. GPS-supported AT produced the stereoscopic viewing accuracy about 0.44 m (ca. 2.93 pixels) in planimetry and 0.55 m (ca. 3.67 pixels) in height. In Taiwan, the planimetric accuracy requirement for 1/5,000 topographic maps is 1.25 m and the vertical accuracy requirement for 1/5,000 topographic maps is 1 m in normal terrain [26]. The test results also imply the following:

1. In this study, non-metric camera is used and calibrated by field method. The test results verify the applicability of the calibrated camera parameters. From the analysis of stereo viewing based on 20 horizontal ground check points and 29 vertical ground check points, although some systematic errors remain, the test results still show that the accuracy of these two indirect georeferencing approaches of fixed-wing UAS images can be used for updating local 1/5,000 topographic maps in Taiwan.
2. This study confirms the feasibility of VBS RTK GPS-supported AT for UAS images. The VBS RTK GPS technique only requires a GPS double frequency carrier receiver to be carried on the UAS for capturing highly accurate and precise flying trajectories. Setting up a physical GPS reference base station on site within the mapping area is unnecessary, especially in inaccessible areas such as mountainous areas; this reduces the ground survey demands placed on GCPs, saving mapping costs and improving mapping efficiency.
3. The non-metric camera installed on the UAS for recording the image data is CMOS sensor. It is not of fiducial marks and is also too small to make precise offset surveys by total station instrument. This study verifies that the GPS antenna-camera offset problem can be overcome by including linear drift parameters in GPS observation equations on each strip, while performing GPS-supported AT for UAS images.
4. Using two cross strips to strengthen block geometry decreases the number of GCPs. Therefore, two cross strips with eight GCPs at the corners of the mapping area are an appropriate GCP configuration for VBS RTK GPS-supported AT for UAS images. This GCP configuration is efficient, especially for inaccessible mapping areas.

ACKNOWLEDGMENTS

This study is sponsored under the grants of the projects NSC 101-2119-M-004-001-. The National Land Surveying and Mapping Center, Taiwan, provided the e-GPS radio instruments. Skyline Dynamics Co. Ltd. and Data Surpass Technology Co. Ltd integrated the VRS GPS receiver hardware. Control Signal Co. Ltd. supported the DGPS post processing technique. The author would like to express hearty gratitude for all of their efforts.

REFERENCES

1. The UAV-The Future Of The Sky. (n.d.). Retrieved March 12, 2016, from http://www.theuav.com/http://www.theuav.com/
2. Eisenbeiss, H., "A mini Unmanned Aerial Vehicle (UAV): System overview and image acquisition," *International Archives of Photogrammetry and Remote Sensing*, Vol. 36, Part-5/W1. (on CD-ROM)(2004).
3. Berni, J., Zarco-Tejada, P., Suárez, L., and Fereres, E., "Thermal and narrowband multispectral remote sensing for vegetation monitoring from an unmanned aerial vehicle," *IEEE Transactions on Geoscience and Remote Sensing*, Vol. 47, No. 3, pp. 722–738 (2009).
4. Lin, Y., Hyyppä, J., and Jaakkola, A., "Mini-UAV-Borne LIDAR for Fine-Scale Mapping," *IEEE Transactions on Geoscience and Remote Sensing*, Vol. 8, No. 3, pp. 426–430 (2011).
5. Eisenbeiss, H., "UAV photogrammetry," PhD Dissertation, DISS. ETH NO. 18515, Institute of Geodesy and Photogrammetry, ETH Zurich, Switzerland (2009).
6. Bendea, H. F., Chiabrando, F., Tonolo, F. G., and Marenchino, D., "Mapping of archaeological areas using a low-cost UAV the Augusta Bagiennorum Test site," *Proc. XXI International CIPA Symposium*, Athens, Greece, 01-06 October. 6p. (on CD-ROM) (2007).
7. Li, S., "The use of low-altitude unmanned aerial vehicle system in the measurement of large scale topographic maps—Take the 1:2,000 mapping of PuWen as an example," *11th South East Asian Survey Congress and 13th International Surveyors' Congress Innovation towards Sustainability*, Malaysia, 8p. (on CD-ROM) (2011).
8. Haarbrink, R. B. and Eisenbeiss, H., "Accurate DSM production from unmanned helicopter systems," *International Archives of Photogrammetry, Remote Sensing and Spatial Information Sciences*, Vol. 37, Part B1, pp. 1259–1264 (2008).
9. Bláha, M., Eisenbeiss, H., Grimm, D. E., and Limpach, P., "Direct georeferencing of UAVs," *Proc. International Conference on Unmanned Aerial Vehicle in Geomatics (UAV-g)*, Zurich, Switzerland, 6 pages. (on CD-ROM) (2011).

10. Chiang, K. W., Tsai, M. L., and Chu, C. H., "The development of an UAV borne direct georeferenced photogrammetric platform for ground control point free applications," *Sensors*, Vol. 12, No. 7, pp. 9161–9180 (2012).
11. Jóźków, G. and Toth, C., "Georeferencing experiments with uas imagery," *ISPRS Annals of the Photogrammetry, Remote Sensing and Spatial Information Sciences*, Volume II-1, 2014, ISPRS Technical Commission I Symposium, Denver, Colorado, USA (2014).
12. Wolf, P. R. and Dewitt, B. A., *Elements of Photogrammetry: With Applications in GIS*, third Ed., The McGraw-Hill, New York (2000).
13. Frieß, P., T. Heuchel "Experience with GPS-supported aerial triangulation," *International Archives of Photogrammetry and Remote Sensing*, ISPRS Commission I, Vol. 29, B1, Washington, D.C., pp. 299–305 (1992).
14. Ackermann, F., "GPS for photogrammetry," *International Society for Photogrammetry and Remote Sensing*, Vol. 56, No. 4, pp. 387–406 (1997).
15. Bilker, M., Honkavaara, E., and Jaakkola, J., "GPS supported aerial triangulation using untargeted ground control," *International Archives of Photogrammetry and Remote Sensing*, Vol. 32, Part 3, pp. 2–9 (1998).
16. Friess, P., "Kinematic GPS positioning for aerial photogrammetry empirical results," *Proc. International Symposium on Precise Positioning with the Global Positioning System*, Ottawa, pp. 1169–1184 (1990).
17. Brown, D. C., "The bundle adjustment-progress and prospects," *International Archives of Photogrammetric and Remote Sensing*, Vol. 21, Part 3, pp. 1–33 (1976).
18. Jedlička, J. and Potůčková, M., "Correction of radial distortion in digital images," *Proceedings Technical Computing Prague*, 5 pages (2006).
19. Lucas, J., "Aerotriangulation without ground control," *Photogrammetric Engineering and Remote Sensing*, Vol. 53, No. 3, pp. 311–314 (1987).
20. DENG Qing-jun, GAO Fei, LI Xiao-li, "Discussion on digital mapping by using the free station method," *Journal of Hefei University of Technology(Natural Science)* 2009-07 (2009). http://en.cnki.com.cn/Article_en/CJFDTotal-HEFE200907030.htm
21. Wang, H. L. and Wang, S. C., "Influence of control patterns on the accuracy of the GPS supported aerial triangulation," *Journal of Photogrammetry and Remote Sensing*, Vol. 3, No. 2, pp. 1–15 (1998).
22. Hinsken, L., Miller, S., Tempelmann, U., Uebbing, R., and Walker, A. S., "Triangulation of the LH systems' ADS40 using ORIMA GPS/IMU," *International Archives of Photogrammetry, Remote Sensing and Spatial Information Sciences*, Vol. 34, Part 3A, pp. 156–162 (2002).
23. Blankenberg, L. E., "GPS supported aerial triangulation-state of the art," *Photogrammetry Journal of Finland*, Vol. 13, No. 1, pp. 4–16 (1992).
24. Ackermann, F., "Operational rules and accuracy models for GPS aerial triangulation," *International Archives of Photogrammetry and Remote Sensing*, Vol. 29, Part B3, pp. 691–700 (1992).
25. Wang, M. S., Liu, C. C., and Lee, Y. H., *Setting a Real-Time Kinametic (RTK) System of National e-GPS Base Staions*, M.O.I. National Land Surveying and Mapping Center, Ed., Taiwan (2006).
26. 內政部國土測繪中心，基本圖測製說明，台中，中華民國 101 年。

104 年 9 月 2 日 收稿
104 年 11 月 21 日 修改
105 年 6 月 15 日 接受